Compensation of the Current-Transformer Saturation Effects for Digital Relays

Firouz Badrkhani Ajaei, Majid Sanaye-Pasand, *Senior Member, IEEE*, Mahdi Davarpanah, Afshin Rezaei-Zare, *Senior Member, IEEE*, and Reza Iravani, *Fellow, IEEE*

***Abstract*—A current transformer (CT) is accurately modeled for representation of the CT saturation effects on digital protective relays. Simulation studies performed in the PSCAD/EMTDC platform are used to investigate the impacts of CT saturation on the current phasor estimation. A new algorithm is also proposed for detection and compensation of CT saturation effects, based on: a least error squares (LES) filter which estimates the phasor parameters of the CT secondary current; a novel saturation detection method which uses the output of the LES filter for saturation detection; and a new minimum estimation error tracking approach which enhances the precision of the phasor estimation. The proposed saturation detection/compensation algorithm is independent of the parameters of the CT, the burden, and the power system. The study results show that the proposed algorithm: 1) reconstructs the distorted current waveform, under dc and ac saturation conditions, with the required precision and speed and 2) performs satisfactorily under inductive burden and under deep and slight saturation conditions.**

***Index Terms*—Current transformer (CT), digital relays, least error squares (LES) method, magnetic saturation, Preisach theory.**

I. Introduction

CURRENT-TRANSFORMER (CT) saturation leads to inaccurate current measurement which may cause malfunction of protective relays [1]. The saturation can be: 1) dc saturation due to the high decaying dc component of the fault current and/or the premagnetization of the CT core and 2) ac saturation due to the large ac current magnitude [2]–[5]. Practically, it is not viable to design a CT not to exhibit dc saturation [6]. AC saturation can be avoided by proper selection of the CT with respect to the maximum anticipated fault current magnitude. However, unforeseen changes in the power system short-circuit capacity (e.g., due to topological changes) may lead to ac saturation of even a properly selected CT.

Thus, a protective relay is practically subject to saturation effects of the corresponding CT which adversely impacts its performance, if appropriate methods for saturation detection and/or compensation are not applied [7]. Several saturation detection/compensation methods, to mitigate the adverse effects of CT saturation on the protection relays, have been proposed in the technical literature. These include:

- Saturation detection techniques to block/unblock the operation of certain protection functions. The main drawback of this approach is the delayed operation and low/inadequate sensitivity [1].
- Reconstructing the distorted CT secondary current based on an approximate CT model [8]–[11]. This is a viable method if the CT burden, winding impedance, and the saturation characteristic are available.
- Reconstructing the CT secondary current using artificial neural networks (ANNs) [2], [12]–[14]. This method necessitates the availability of a vast amount of training data [15] and, hence, cannot be universally applied due to the variations of burden and CT characteristics [7], [16].
- Estimation of the current phasor parameters from the unsaturated portions of the current waveform [1], [7], [8], [17], [18]. This approach needs an effective saturation detection technique for accurate identification of the unsaturated portions of the measured current waveform [1].

The majority of the existing saturation detection techniques [8], [17], and [18] cannot reliably identify the saturation termination instant [2] and [19], especially under inductive burden conditions [1]. The reason is that these methods generally depend on the changes of the CT secondary current, which is smoother under inductive burden conditions [2], [19]. Furthermore, some of these methods [8], [17] need the maximum fault current magnitude and, thus, their performances depend on the power system topology.

An accurate magnetic core characteristic model based on the Preisach theory [20], adopted for a 300/1 A 5P20 class CT, is used for precise simulation of CT saturation. The adopted CT model represents minor loops, remanent flux, and eddy current effects. Considering the shortcomings of the existing methods, an efficient algorithm for the detection and compensation of CT saturation effects is proposed to be used in digital protective distance and overcurrent relays in transmission and subtransmission systems. A least error squares (LES) filter [21] with a short sliding data window is used for phasor parameters estimation during unsaturated portions of the CT output current waveform.

Manuscript received November 15, 2010; revised March 31, 2011; accepted June 29, 2011. Date of publication August 18, 2011; date of current version October 07, 2011. Paper no. TPWRD-00875-2010.

F. B. Ajaei, and M. Davarpanah are with the Electrical and Computer Engineering School, College of Engineering, University of Tehran, Tehran 14395-515, Iran (e-mail: f.badrkhani@ece.ut.ac.ir; m.davarpanah@ut.ac.ir).

M. Sanaye-Pasand is with the Electrical and Computer Engineering School, College of Engineering, University of Tehran, Tehran 14395-515, Iran. He is also with the Control and Intelligent Processing Center of Excellence, Electrical and Computer Engineering School, University of Tehran, Tehran 14395-515, Iran.(e-mail: msanaye@ut.ac.ir).

A. Rezaei-Zare and R. Iravani are with the Department of Electrical and Computer Engineering, University of Toronto, Toronto, ON M5S 3G4, Canada (e-mail: a.rezaei@utoronto.ca; iravani@ecf.utoronto.ca).

Color versions of one or more of the figures in this paper are available online at http://ieeexplore.ieee.org.

Digital Object Identifier 10.1109/TPWRD.2011.2161622

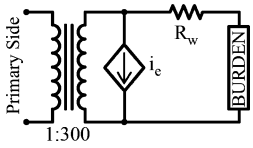

Fig. 1. CT model used for simulation studies.

The unsaturated portions are detected using the proposed saturation detection method based on the convergence of the estimated current magnitude. Unlike most of the existing CT saturation detection algorithms, the proposed method exhibits high sensitivity in detecting deep and slight saturation, even under inductive burden conditions. In addition, a minimum estimation error tracking (MEET) approach is introduced to increase the precision of the phasor estimation during the detected unsaturated portions of the current waveform.

The proposed saturation detection/compensation algorithm has a fast response. Its performance is independent of the power system topology, the CT parameters and characteristics, and the burden. Thus, it does not require any pre-specified threshold values based on these factors. It is simple and, thus, suitable for online implementation and has no cumulative estimation errors. Moreover, it is able to reconstruct the fundamental frequency component of the distorted CT secondary current waveform, under ac and dc saturation conditions, and it is secure against permissible levels of current harmonics. The CT model and the saturation compensation algorithm are implemented and tested in the PSCAD/EMTDC software environment.

II. CT Model

Fig. 1 shows a schematic diagram of the investigated CT, where i_e and R_w denote the excitation current and the winding resistance, respectively. Table I provides the CT data. The excitation current of the CT magnetic core is

$$i_e = i_h + i_{\text{eddy}} \tag{1}$$

where i_h is the hysteresis current and determined based on the Preisach hysteresis model, and i_{eddy} is the eddy current

$$i_{\text{eddy}} = \sigma_e \times v_e \tag{2}$$

where $\sigma_e = 8 \times 10^{-4}\ \Omega^{-1}$ is the eddy current factor of the laminations [22], and v_e is the excitation voltage. The total core flux density B consists of two parts

$$B(H) = B_{hys}(H) + B_{sat}(H) \tag{3}$$

where H is the core magnetic field intensity. $B_{\text{hys}}(H)$ is the flux density corresponding to the hysteresis component of the magnetization characteristic, defined by the Preisach theory. Meanwhile, $B_{\text{sat}}(H)$ is a linear single-valued function which describes the flux density in the saturation region as

$$B_{\text{sat}}(H) = \frac{l_c}{N_s^2 A} L_{\text{sat}} H \tag{4}$$

TABLE I
CT Parameters

Turn ratio	300/1
Fundamental frequency	50 Hz
Mean core length	0.448 m
Cross section area	0.00168 m^2
Winding resistance	2.1 Ω
Air core inductance	0.85 mH
Saturation flux density	1.88 T
Nominal burden	8 VA

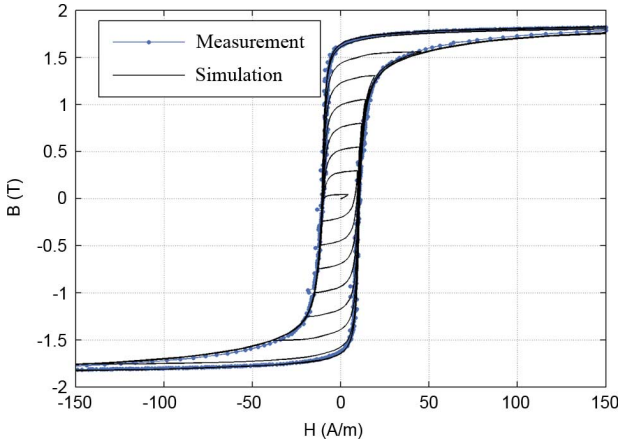

Fig. 2. Major and minor hysteresis loops of the studied CT.

where L_{sat}, N_s, l_c, and A denote the air-core inductance, the number of secondary turns, the core mean flux path length, and the effective core cross section area, respectively [23].

The hysteresis loops of the CT are measured using a low frequency (1 Hz) sinusoidal excitation voltage to minimize the effects of the stray capacitances. Using the method introduced in [23]–[28], the measured hysteresis loops data are used to identify the Everett function [29], which defines the hysteresis loops for the Preisach model. Numerical implementation of the Preisach model (i.e., determination of the magnetic flux density B as a function of the field intensity H) is illustrated in [30]–[32]. The value of i_h in each sampling period is determined by an iterative method adopted to solve the system equations.

Fig. 2 depicts the measured points of the major loop and the simulated minor and major loops, when the field intensity H is assumed to be a sinusoidal signal with an increasing magnitude. This figure demonstrates that the CT core magnetization characteristic is accurately represented.

III. Investigation of the Saturation Effects

In this paper, the fault current is described by

$$i = I_{\text{DC}} \times e^{-t/\tau} + I_m Cos(\omega t + \theta) \tag{5}$$

where I_m, θ, and ω denote the magnitude, phase angle, and fundamental frequency of the current phasor, respectively. I_{DC} and τ denote the magnitude and time constant of the decaying dc component (dc offset), respectively. To develop an appropriate

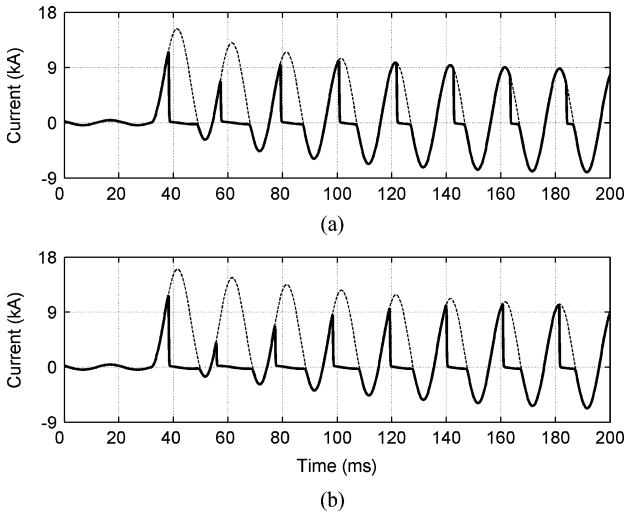

Fig. 3. Primary current (dashed line), and scaled secondary current (solid line) of the CT. (a) $\tau = 50$ ms and (b) $\tau = 100$ ms.

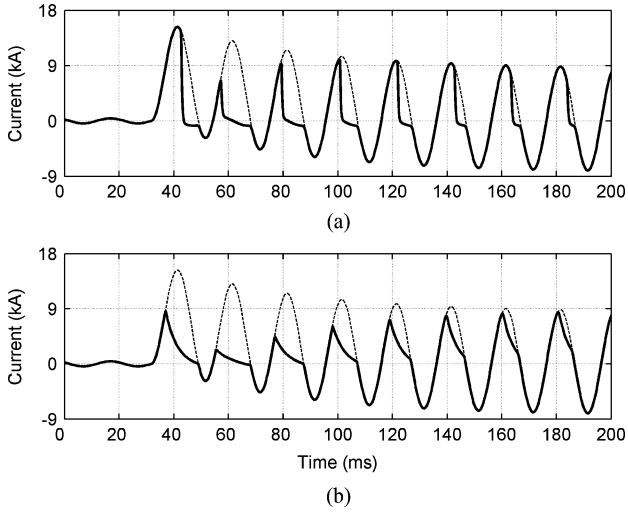

Fig. 4. Repetition of Fig. 3(a) when the CT carries (a) 1 Ω resistive burden and (b) 8 Ω burden at the power factor of 0.5.

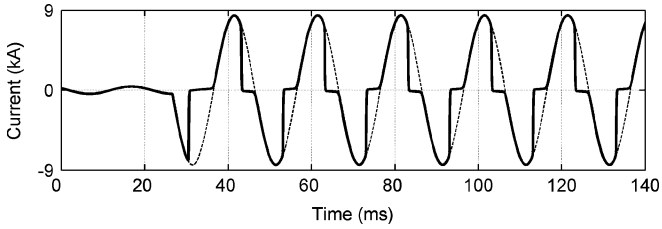

Fig. 5. Primary current (dashed line), and scaled secondary current (solid line) of the CT corresponding to a 12 Ω resistive burden.

algorithm for compensating CT saturation effects, various parameters that may affect the saturation must be considered. According to [12], these parameters include I_m, τ, the impedances of the secondary winding, the burden, the remanent flux, and the fault incidence angle which determines the value of $I_{\rm DC}$.

A. DC Saturation

DC saturation of a current transformer is caused by a dc component in the CT primary current (e.g., the decaying dc component of the fault current). This type of saturation is often encountered, since the fault current usually contains a considerable decaying dc component.

1) Effects of the Decaying DC Component: An asymmetrical fault current can saturate a CT at much smaller current than a symmetrical current [12]. To investigate the effect of the decaying dc component on CT saturation, a short-circuit event with the current magnitude of 6 kA rms (20 times the nominal current) and with the maximum decaying dc component is considered. The CT carries its 8 Ω nominal burden at the unity power factor. Fig. 3(a) and (b) depicts the primary and the scaled secondary currents of the CT, when the time constant of the decaying dc component is set at 50 ms and 100 ms, respectively. Fig. 3 illustrates that a higher decaying dc time constant results in deeper CT saturation. Fig. 3 also illustrates that during dc saturation, the CT output current waveform includes only one saturated portion per cycle. The reason is that the flux reaches the knee point only in one direction during dc saturation.

2) Effects of Burden: To investigate the effect of the burden on dc saturation, the short-circuit event shown in Fig. 3(a) is repeated with a lower burden value of 1 Ω [Fig. 4(a)] and a lower power factor of 0.5 [Fig. 4(b)]. The CT primary current is the same for the results shown in Figs. 3(a) and 4. Comparing the simulation results of Fig. 4 with those of Fig. 3(a), one concludes that during dc saturation 1) a higher burden results in deeper saturation and 2) a lower power factor of the burden results in a smoother CT output current waveshape.

B. AC Saturation

AC saturation of a CT is caused by a high fault current magnitude or a high burden impedance. Although a digital relay introduces a low burden impedance to the CT, a high wiring impedance may cause this type of saturation [33]. To investigate the ac saturation effects, a 6-kA short-circuit event without a decaying dc component is considered. Fig. 5 depicts the primary and the scaled secondary currents of the CT for a 12 Ω resistive burden (i.e., 150% of the nominal value). Fig. 5 demonstrates that, during ac saturation, the CT output current waveform includes two saturated and two unsaturated intervals per cycle.

C. Impacts of CT Saturation on Phasor Estimation

The performance of a full-cycle fast Fourier transform under CT saturation conditions is investigated. The estimated phasor parameters of the primary and the scaled secondary currents of the CT, subjected to the dc saturation of Fig. 3(a) and the ac saturation of Fig. 5, using a 20-sample Fourier filter, are depicted in Figs. 6 and 7, respectively. These figures illustrate that dc and ac saturation phenomena result in inaccurate estimation of the magnitude and phase of the fault current phasor.

IV. Proposed Saturation Compensation Method

The proposed saturation compensation method is comprised of a fast digital filter to estimate the current phasor parameters

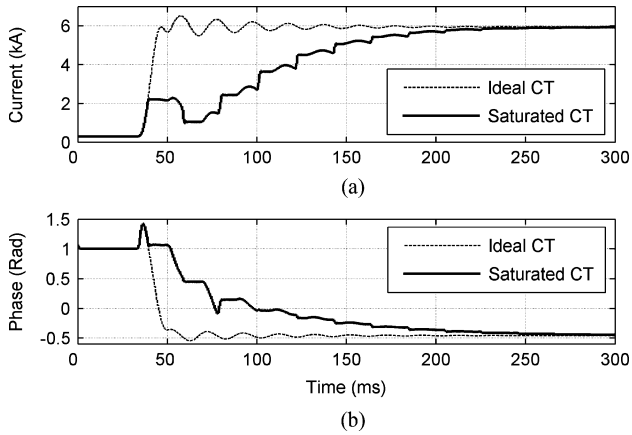

Fig. 6. Estimated (a) magnitude and (b) phase of the scaled secondary current of the CT, using the Fourier filter, during the short circuit of Fig. 3(a).

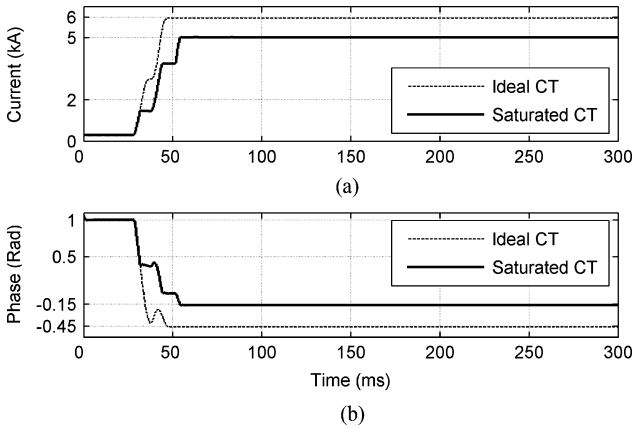

Fig. 7. Estimated (a) magnitude and (b) phase of the scaled secondary current of the CT, using the Fourier filter, during the short circuit of Fig. 5.

during the unsaturated portions of the current waveform, and an algorithm which detects and reconstructs the saturated portions.

A. Utilized Digital Filter

An LES digital filter with decaying dc component extraction capability [21] is used for the estimation of the current phasor magnitude and phase angle. A short data window length (3 ms) is chosen for accurate phasor parameters estimation by using the unsaturated portions of the current waveform. The sampling frequency of the LES filter is 4 kHz.

A CT saturation compensation algorithm must quickly and accurately estimate the current phasor parameters under various saturation conditions. Hence, the proposed saturation detection/compensation method is developed considering the impacts of both dc and ac saturation conditions.

1) Impacts of DC Saturation on the LES Filter: Fig. 8 shows the estimated fault current magnitude using the LES filter, during the short-circuit event of Fig. 3(a), and indicates that the estimated magnitude is different when compared to the output of the Fourier filter [Fig. 6(a)]. Fig. 9 shows the scaled CT output current and its estimated magnitude, for one cycle of the fundamental frequency during the dc saturation of Fig. 3(a). Fig. 9 illustrates that the estimated magnitude is erroneous and unstable (i.e., it does not converge to a constant

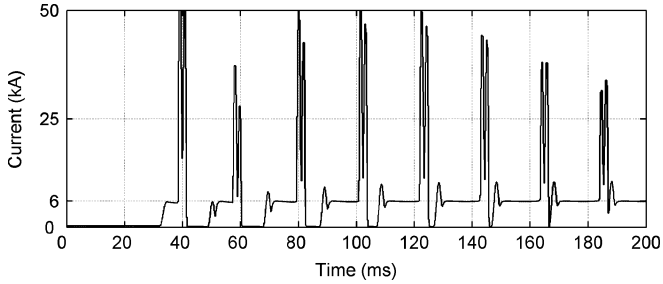

Fig. 8. Estimated fault current magnitude with the LES filter during the short-circuit event of Fig. 3(a).

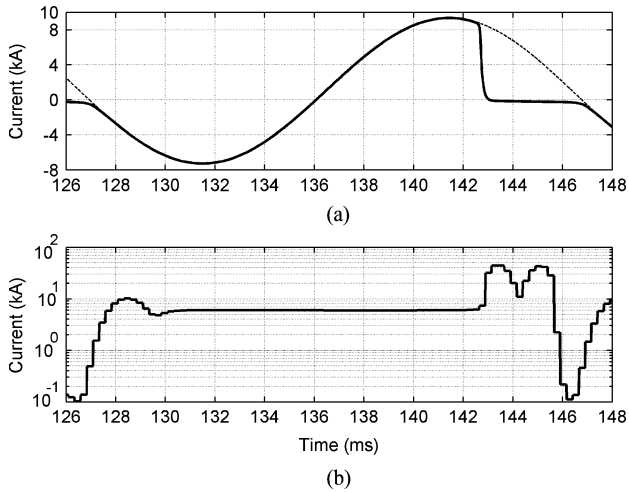

Fig. 9. (a) Primary (dashed line) and scaled secondary (solid line) currents of the CT. (b) Estimated current magnitude by the LES filter.

value, during the saturated portion of the waveform $(143 < \mathrm{t} < 147$ ms). Besides, it shows that during the unsaturated portion $(127 < \mathrm{t} < 143\ \mathrm{ms})$, the estimated current magnitude is stable (i.e., converges to 6 kA), as the transition time of the LES filter (data window length of 3 ms) expires. Thus, the phasor is accurately estimated during the interval of $130 < \mathrm{t} < 143$ ms.

2) Impacts of AC Saturation on the LES Filter: For the ac saturation event of Fig. 5, the scaled CT output current and its estimated magnitude during one cycle of the fundamental frequency are shown in Fig. 10. This figure illustrates that the estimated current magnitude is unstable during the saturated portions of the current waveform ($133 < \mathrm{t} < 137$ ms and $143 < \mathrm{t} < 147$ ms). Moreover, it shows that during the unsaturated portions ($127 < \mathrm{t} < 133$ ms and $137 < \mathrm{t} < 143$ ms), the estimated current magnitude becomes stable as the 3-ms transition time of the LES filter expires ($130 < \mathrm{t} < 133$ ms and $140 < \mathrm{t} < 143$ ms).

B. Proposed Saturation Detection Algorithm

Figs. 9 and 10 demonstrate that a sampled portion of the current waveform can be assumed sinusoidal when the estimated current magnitude converges to a constant value (i.e., the filter output becomes stable). Accordingly, we propose a new saturation detection approach which detects the unsaturated portions of the current waveform by assessing the stability of the LES filter output. The average deviation of the estimated magnitudes of the CT secondary current is a reasonable filter output stability

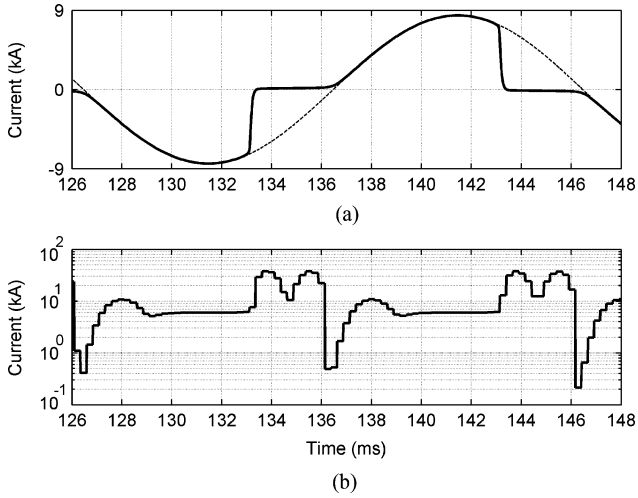

Fig. 10. (a) Primary (dashed line) and scaled secondary (solid line) currents of the CT. (b) Estimated current magnitude by the LES filter.

index. However, the value of the average deviation depends on the current magnitude. Therefore, the normalized average deviation (NAD) of the last eight estimated magnitudes is used as the output stability indicator of the LES filter (i.e., the saturation detection index) and defined by

$$\mathrm{NAD} = \frac{\left(\frac{1}{8}\sum_{i=-7}^{0}\left|M_i - \bar{M}\right|\right)}{\bar{M}}, \quad \bar{M} = \frac{1}{8}\sum_{i=-7}^{0} M_i \qquad (6)$$

where M_i, $i = -7 \ldots 0$ denotes the last ith estimated magnitude.

During the sinusoidal portions of the current waveform, the NAD value approaches to zero. Therefore, the sinusoidal portions can be detected when the NAD value becomes less than a prespecified threshold. However, the study results indicated that the CT secondary current is sinusoidal not only during the unsaturated portions, but also during the deeply saturated portions. The reason is that at considerably high excitation currents, the CT core characteristic is almost linear since the air-core inductance of the CT is almost constant. Thus, during the deeply saturated portions, the excitation current is sinusoidal which results in a sinusoidal CT secondary current with a very low magnitude. This phenomenon is shown in Fig. 11 [magnification of Fig. 3(a)], during the interval of $58 < \mathrm{t} < 68$ ms. Under deep saturation conditions, the output of the LES filter becomes stable after its transition time period expires $61 < \mathrm{t} < 68$ ms in Fig. 11(b), and results in a low NAD value [Fig. 11(c)].

Thus, one concludes that the calculated NAD becomes less than the threshold value (i.e., the sampled current waveform portion is sinusoidal), when:

1) the CT is not saturated under normal operation conditions;
2) the CT is not saturated under short-circuit conditions;
3) the CT is saturated during a short-circuit event, and the sampled portion is an unsaturated portion of the CT secondary current waveform ($73 < \mathrm{t} < 79$ ms in Fig. 11);
4) the CT is saturated during a short-circuit event, and the sampled portion is a deeply saturated portion of the CT secondary current waveform ($62 < \mathrm{t} < 68$ ms in Fig. 11).

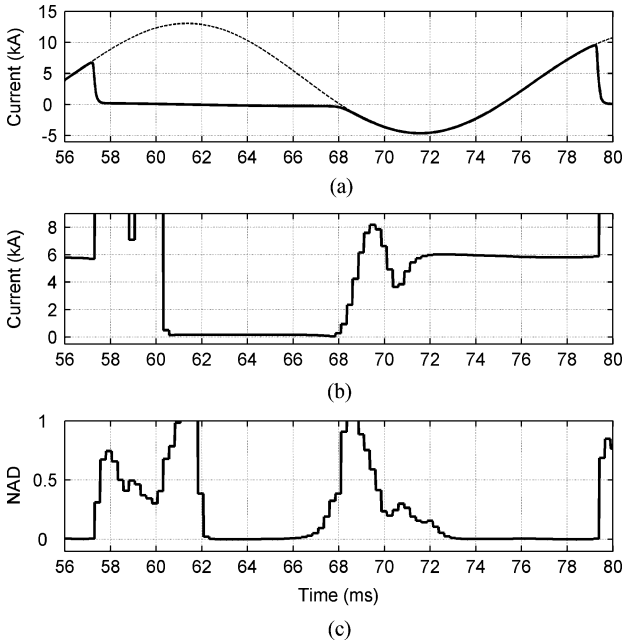

Fig. 11. (a) Primary current (dashed line), and scaled secondary current (solid line) of the CT. (b) Estimated current magnitude by the LES filter. (c) NAD of the estimated magnitude.

Fig. 11(b) shows that the case 4 results in a very low estimated magnitude (lower than twice the magnitude of the nominal CT secondary current I_n). Moreover, it never lasts for one cycle. Hence, to make a distinction between these cases, the last estimated magnitude M_0 and the duration of the detected portion with low estimated magnitude, denoted by T_{low}, are considered. Therefore, based on the proposed saturation detection algorithm, the sampled current waveform portion is unsaturated when one of the following terms is satisfied:

- $((\mathrm{NAD}<0.1)\ \&\ (M_0<2\times I_n)\ \&\ (T_{\mathrm{low}}>20\,\mathrm{ms}))$, $\rightarrow$ case 1;
- $((\mathrm{NAD}<0.1)\ \&\ (M_0>2\times I_n))$, $\rightarrow$ case 2 or 3

and saturated or highly distorted when one of the following is satisfied:

- $((\mathrm{NAD}<0.1)\ \&\ (M_0<2\times I_n)\&(T_{\mathrm{low}}<20\,\mathrm{ms}))$, $\rightarrow$ case 4
- $(\mathrm{NAD}>0.1)$. $\rightarrow$ saturated or distorted signal.

The value of the NAD threshold depends on one hand on the permissible harmonic and noise levels and on the other hand on the maximum acceptable estimation error. A compromise must be made between these two factors. The performed simulation studies indicated that a NAD threshold value of 0.1 results in desirable performance of the algorithm.

The output of the proposed saturation detection algorithm (i.e., the indicator of unsaturated portions) is the "*UNSAT*" signal. Its value is set at 1 when the algorithm assumes that the sampled portion of the current waveform is not saturated, and the estimated current phasor parameters can be used by a digital relay. Otherwise, the *UNSAT* signal is set at 0.

The performance of the proposed saturation detection algorithm is investigated considering a 6 kA short-circuit event with the maximum decaying dc component and time constant of 40 ms. The CT carries a pure resistive burden of 12 Ω. The obtained results shown in Fig. 12 indicate that dc saturation occurs

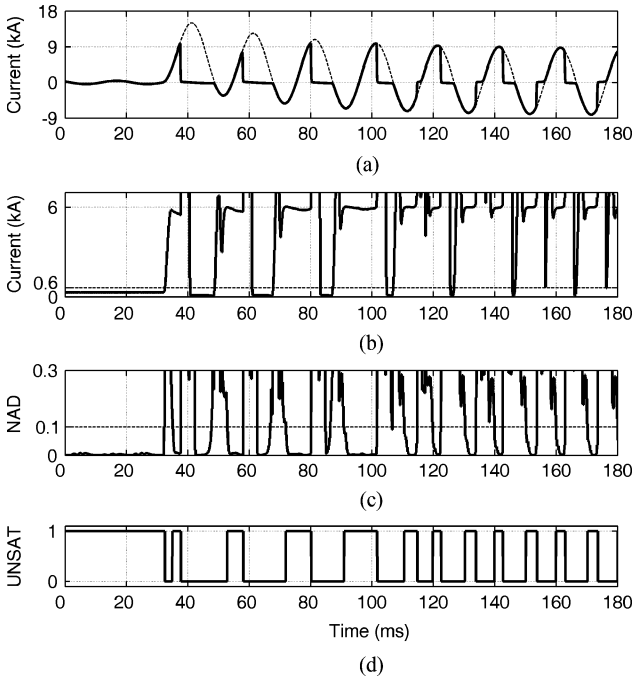

Fig. 12. (a) Primary current (dashed line), and scaled secondary current (solid line) of the CT. (b) Estimated current magnitude by the LES filter (solid line) and the corresponding threshold (dashed line). (c) NAD of the estimated magnitude (solid line) and the corresponding threshold (dashed line). (d) Indicator of the unsaturated segments.

during the first four cycles after the fault initiation and gradually changes to ac saturation [Fig. 12(a)]. The estimated current magnitude and the corresponding threshold ($2 \times I_n = 0.6$ kA) are compared in Fig. 12(b). The calculated NAD and its threshold value of 0.1 are compared in Fig. 12(c). The *UNSAT* signal is shown in Fig. 12(d).

Fig. 12 illustrates that the proposed saturation detection algorithm performs satisfactorily under both dc and ac saturation conditions. As shown in Fig. 12(c), during the unsaturated portions of the current waveform, the calculated NAD becomes less than the prespecified threshold value, after the transition times of the LES filter (3 ms) and the NAD calculation algorithm (2 ms) expire. Accordingly, the proposed algorithm can detect an unsaturated interval which is at least 5 ms, and can be used for reconstructing the CT secondary current waveform under deep saturation conditions.

C. Proposed Reconstruction Algorithm

Assume the estimated magnitude and phase angle of the current phasor in each sampling period using the LES filter are denoted by M_0 and θ_0, respectively. The outputs of the reconstruction algorithm (i.e., the compensated estimates of the current magnitude and phase) are denoted by M_{out} and θ_{out}, respectively. The proposed reconstruction algorithm is described as follows.

The operation of the reconstruction algorithm includes "REFRESH" and "HOLD" modes. In the REFRESH mode, the sampled portion is unsaturated and the estimated phasor parameters are accurate. Thus, the instantaneous estimated variables (M_0 and θ_0) are directly assigned to the output of the algorithm

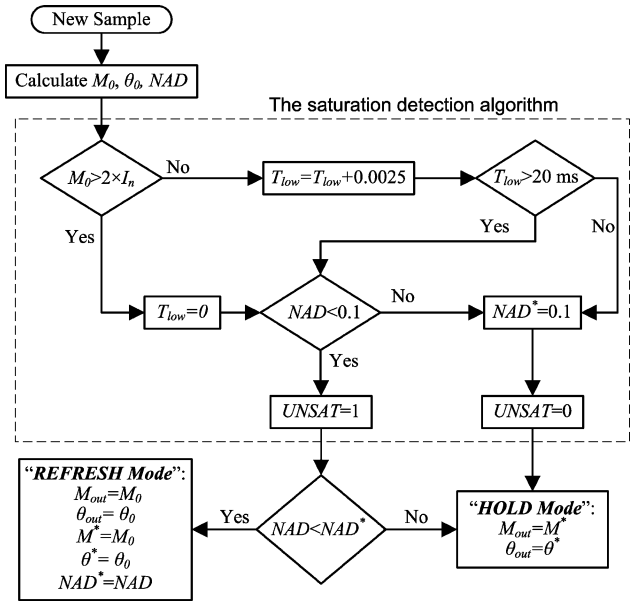

Fig. 13. Flowchart of the proposed CT saturation detection/compensation algorithm.

(M_{out} and θ_{out}). In the HOLD mode, the sampled portion is saturated or highly distorted, and M_{out} and θ_{out} are kept unchanged at the values of the last REFRESH operation.

To determine the operation mode of the reconstruction algorithm, first, the value of the *UNSAT* signal must be set. Accordingly, in each sampling period, if the sampled portion is not unsaturated (i.e., the value of the *UNSAT* signal is 0), the algorithm activates the HOLD mode. Otherwise, the REFRESH mode is activated. Using this approach, during the saturated or highly distorted portions of the current waveform and the transition time of the digital filter, the HOLD mode prevents inaccurate estimation of the phasor parameters.

During the unsaturated portions, the algorithm outputs should not be necessarily refreshed in each sampling period. The study results demonstrated that during these intervals, a lower NAD value corresponds to more precisely estimated phasor parameters. Therefore, to achieve a higher estimation accuracy, a MEET approach is introduced in the reconstruction algorithm. Based on this approach, during each unsaturated portion, the REFRESH mode is activated only in the sampling periods which have lower NAD values compared with the NAD value of the last REFRESH operation. Therefore, after a REFRESH operation in the first sampling period of each unsaturated portion, any subsequent REFRESH operation results in a more precisely estimated set of parameters. It must be noted that the internal variables M^*, θ^*, and NAD^* are used to store the outputs of the algorithm (M_{out} and θ_{out}), and the calculated NAD value, respectively, during the last REFRESH operation. Fig. 13 depicts the flowchart of the proposed saturation detection/compensation algorithm.

V. Performance of the Algorithm

The performance of the proposed CT saturation detection/compensation algorithm is evaluated under various saturation conditions and in the presence of current harmonics. The results

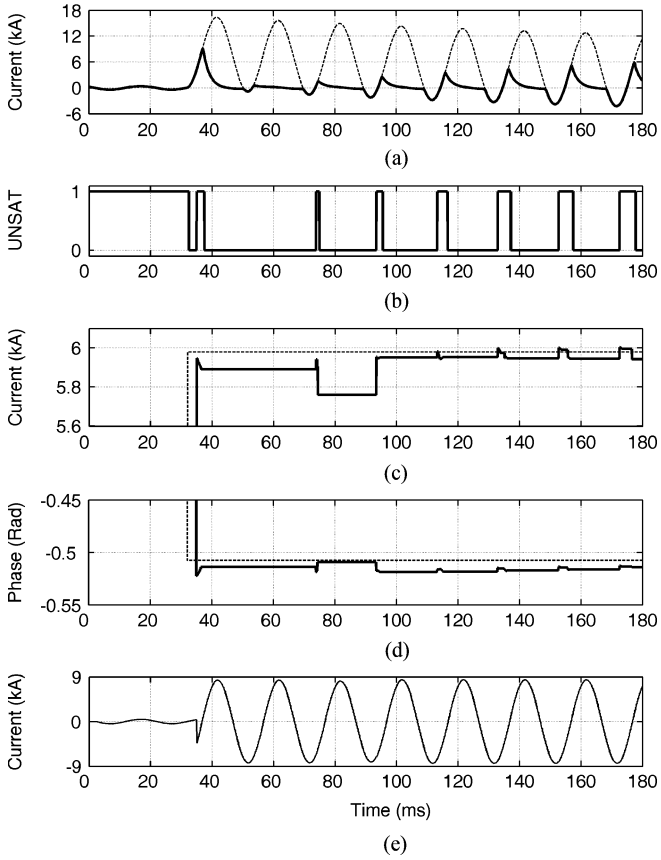

Fig. 14. (a) Primary current (dashed line) and scaled secondary current (solid line) of the CT. (b) Indicator of unsaturated segments. (c) Estimated (solid line) and actual values (dashed line) of the magnitude. (d) Estimated (solid line) and actual values (dashed line) of the phase angle. (e) Reconstructed current waveform.

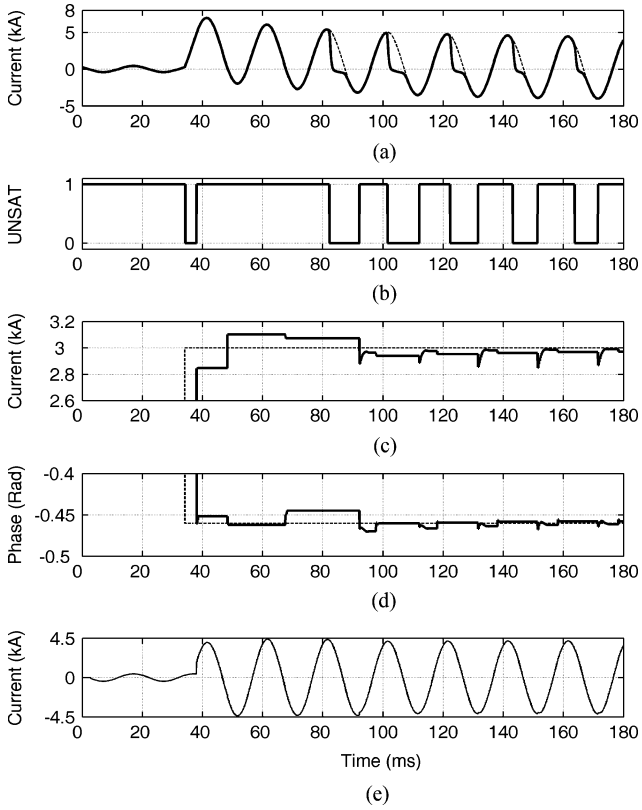

Fig. 15. (a) Primary current (dashed line), and scaled secondary current (solid line) of the CT. (b) Indicator of unsaturated segments. (c) Estimated (solid line) and actual values (dashed line) of the magnitude. (d) Estimated (solid line) and actual values (dashed line) of the phase angle. (e) Reconstructed current waveform.

of the performed simulation studies in the PSCAD/EMTDC platform are presented in this section.

A. CT Saturation Detection/Compensation

Fig. 14 illustrates the performance of the proposed saturation detection and compensation algorithm, under inductive burden and high decaying dc time constant (i.e., deep dc saturation, conditions). Fig. 14(a) shows that under a $8\ \Omega$ burden at the power factor of 0.8, the CT is highly saturated by the 6 kA fault current (time-constant of 200 ms). Fig. 14(b) illustrates that the saturation detection algorithm prevents erroneous phasor estimation at highly saturated cycles (e.g., the second cycle after the fault initiation). The estimated and the actual values of the fault current phasor parameters are shown in Fig. 14(c) and (d), which indicate that the current phasor magnitude and phase angle are estimated in 3.5 ms with less than 4% and 0.011 rad errors, respectively. Fig. 14(e) depicts the corresponding reconstructed fault current waveform and shows that the proposed phasor estimation method does not reconstruct the decaying dc component of the fault current. It should be noted that the level of the decaying dc component is seldom used in protection relays [7].

Fig. 15 depicts the performance of the proposed saturation compensation algorithm under a slight saturation condition while the CT carries a resistive burden of $0.5\ \Omega$ and the fault current magnitude is 3 kA (time-constant of 50 ms). Fig. 15(b) illustrates that the proposed saturation detection algorithm is also effective under slight saturation conditions ($140 < t < 180$ ms). Fig. 15(c) and (d) shows that the magnitude and phase angle of the fault current are estimated in 4 ms with less than 5% and 0.015 rad errors, respectively.

Fig. 16 shows the performance of the proposed reconstruction algorithm during the ac saturation case shown in Fig. 5. Fig. 16 demonstrates that the proposed algorithm performs satisfactorily under ac saturation conditions, and the fault current magnitude and phase angle are estimated in 3.8 ms with less than 4% and 0.05 rad errors, respectively. It must be noted that the estimation error values are the maximum values encountered at the first cycle after the fault initiation. As shown in Figs. 14–16, the estimation errors become smaller at the subsequent cycles.

The performance of the proposed algorithm during an evolving fault is also investigated. A 3 kA rms single-phase-to-ground fault without a decaying dc component occurs at $t = 27$ ms. Subsequently, at $t = 96$ ms, it changes to a 6 kA rms three-phase-to-ground fault including a decaying dc component with a time constant of 100 ms. The obtained simulation results are shown in Fig. 17. This figure illustrates that the proposed algorithm detects the fault-type change and refreshes the estimated phasor parameters in 4 ms, as soon as the transition time of the algorithm expires. The current waveform is reconstructed satisfactorily (i.e., with magnitude and phase errors of less than 4% and 0.1 rad).

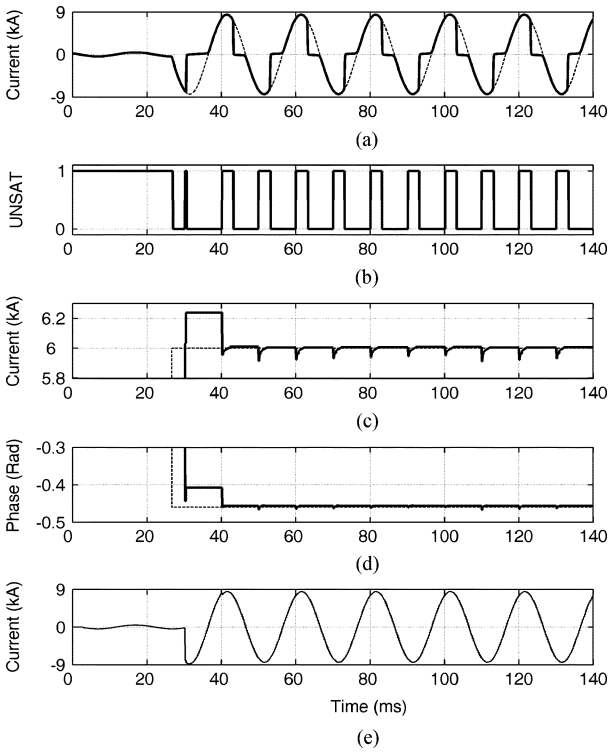

Fig. 16. (a) Primary current (dashed line) and scaled secondary current (solid line) of the CT. (b) Indicator of unsaturated segments, (c) Estimated (solid line) and actual values (dashed line) of the magnitude. (d) Estimated (solid line) and actual values (dashed line) of the phase angle. (e) Reconstructed current waveform.

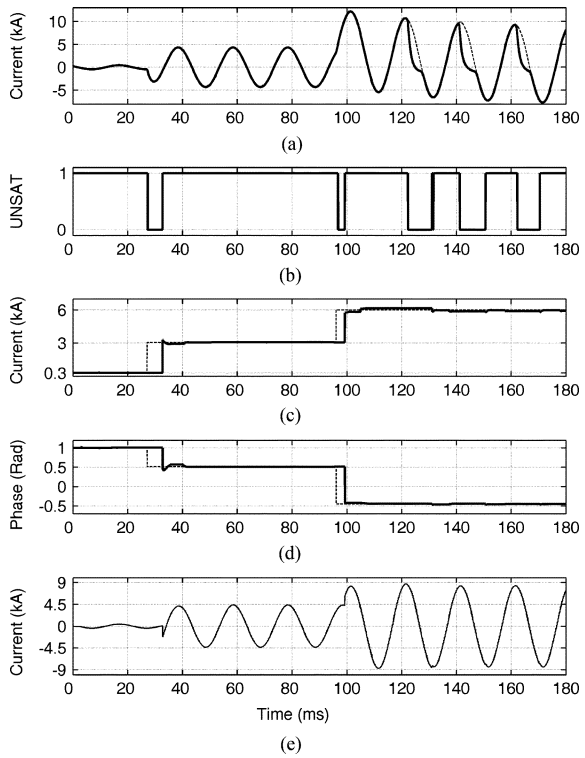

Fig. 17. (a) Secondary current of the CT. (b) Indicator of unsaturated segments. (c) Estimated (solid line) and actual values (dashed line) of the magnitude. (d) Estimated (solid line) and actual values (dashed line) of the phase angle. (e) Reconstructed current waveform.

B. Current Harmonics Effects

According to the standard [34] for the systems with voltage levels higher than 69 kV, where the proposed algorithm is intended to be utilized, the maximum-permissible magnitude of the current odd harmonics is 2% for the harmonics of orders lower than 11, and 1% for the harmonics of orders between 11 and 17. In order to evaluate the performance of the proposed algorithm in the presence of harmonics, the odd harmonics of orders lower than 17, with the aforementioned maximum permissible levels, are added to the current signal under normal operation conditions. Fig. 18 shows the performance of the algorithm in the presence of current harmonics. As shown in Fig. 18(c) and (d), the algorithm estimates the current phasor magnitude and phase with less than 4% and 0.05 rad errors, respectively. Fig. 18(e) shows that the reconstructed current waveform is less distorted than the original current waveform. This figure demonstrates that the MEET approach significantly increases the precision of the phasor estimation.

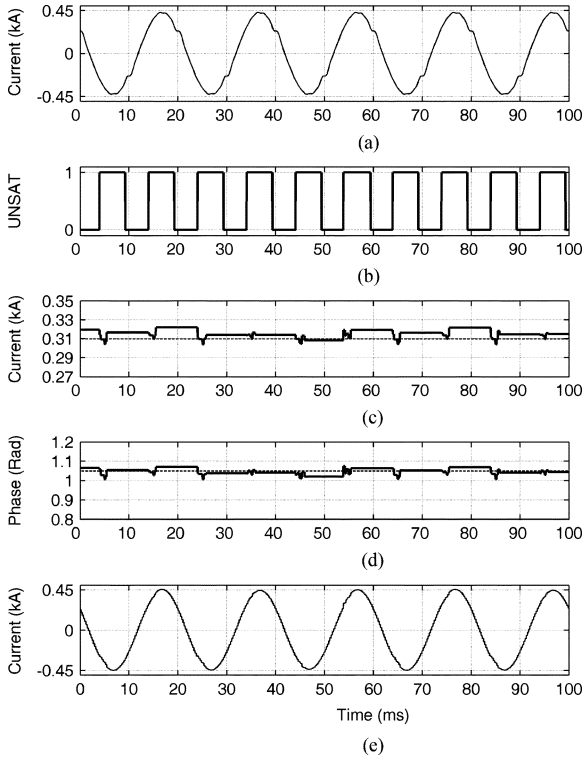

Fig. 18. (a) Secondary current of the CT. (b) Indicator of unsaturated segments. (c) Estimated (solid line) and actual values (dashed line) of the magnitude. (d) Estimated (solid line) and actual values (dashed line) of the phase angle. (e) Reconstructed current waveform.

VI. Conclusion

Using a detailed CT model that accurately represents the CT saturation effects, a new algorithm was introduced to compensate for the impacts of CT saturation on digital relays. The algorithm, which reconstructs the distorted secondary currents of saturated CTs, comprises novel saturation detection and compensation methods. The former detects the unsaturated portions of the CT secondary current by assessing the convergence of the estimated current magnitude. The latter compensates the saturation effects using the estimated phasor parameters based on

the unsaturated portions of the current waveform. A minimum estimation error tracking approach was also introduced, which considerably enhances the precision of the phasor estimation.

The performance of the proposed algorithm was investigated through several simulation studies in the PSCAD/EMTDC software environment. The study results indicated that the proposed algorithm reconstructs the saturated CT secondary current in about 4 ms with acceptable magnitude and angle errors, under deep and slight saturations of ac and dc types.

REFERENCES

[1] J. Pan, K. Vu, and Y. Hu, "An efficient compensation algorithm for current transformer saturation effects," *IEEE Trans. Power Del.*, vol. 19, no. 4, pp. 1623–1628, Oct. 2004.

[2] W. Rebizant and D. Bejmert, "Current-transformer saturation detection with genetically optimized neural networks," *IEEE Trans. Power Del.*, vol. 22, no. 2, pp. 820–827, Apr. 2007.

[3] L. J. Powell, "Current transformer burden and saturation," *IEEE Trans. Ind. Appl.*, vol. IA-15, no. 3, pp. 294–303, May/Jun. 1979.

[4] B. Kasztenny and D. Finney, "Generator protection and CT-saturation problems and solutions," *IEEE Trans. Ind. Appl.*, vol. 41, no. 6, pp. 1452–1457, Nov./Dec. 2005.

[5] P. Chawande, S. A. Soman, P. R. Apte, and S. Pandit, "Experimental evaluation of current transformer performance under saturation," in *Proc.7th Int. Power Eng. Conf.*, Singapore, 2005, pp. 1–5.

[6] P. K. Gangadharan, T. S. Sidhu, and G. J. Finlayson, "Current transformer dimensioning for numerical protection relays," *IEEE Trans. Power Del.*, vol. 22, no. 1, pp. 108–115, Jan. 2007.

[7] A. Wiszniewski, W. Rebizant, and L. Schiel, "Correction of current transformer transient performance," *IEEE Trans. Power Del.*, vol. 23, no. 2, pp. 624–632, Apr. 2008.

[8] Y. C. Kang, U. J. Lim, S. H. Kang, and P. A. Crossley, "Compensation of the distortion in the secondary current caused by saturation and remanence in a CT," *IEEE Trans. Power Del.*, vol. 19, no. 4, pp. 1642–1649, Oct. 2004.

[9] Y. C. Kang, J. K. Park, S. H. Kang, A. T. Johns, and R. K. Aggarval, "An algorithm for compensating secondary currents of current transformers," *IEEE Trans. Power Del.*, vol. 12, no. 1, pp. 116–124, Jan. 1997.

[10] N. Locci and C. Muscas, "A digital compensation method for improving current transformer accuracy," *IEEE Trans. Power Del.*, vol. 15, no. 4, pp. 1104–1109, Oct. 2000.

[11] S. Bittanti, F. A. Cuzzola, F. Lorito, and G. Poncia, "Compensation of nonlinearities in a current transformer for the reconstruction of the primary current," *IEEE Trans. Control Syst. Technol.*, vol. 9, no. 4, pp. 565–573, Jul. 2001.

[12] H. Khorashadi-Zadeh and M. Sanaye-Pasand, "Correction of saturated current transformers secondary current using ANNs," *IEEE Trans. Power Del.*, vol. 21, no. 1, pp. 73–79, Jan. 2006.

[13] D. C. Yu, J. C. Cummins, Z. Wang, H. J. Yoon, and L. A. Kojovic, "Correction of current transformer distorted secondary currents due to saturation using artificial neural networks," *IEEE Trans. Power Del.*, vol. 16, no. 2, pp. 189–194, Apr. 2001.

[14] Y. Y. Hong and P. C. Chang-Chian, "Detection and correction of distorted current transformer current using wavelet transform and artificial intelligence," *Inst. Eng. Technol. Gen. Transm. Distrib.*, vol. 2, no. 4, pp. 566–575, 2008.

[15] P. Stachel and P. Schegner, "Detection and correction of current transformer saturation effects in secondary current signals," in *Proc. IEEE Power Eng. Soc. Gen. Meeting*, Canada, 2009, pp. 1–6.

[16] Z. Lu, J. S. Smith, and Q. H. Wu, "Morphological lifting scheme for current transformer saturation detection and compensation," *IEEE Trans. Circuits Syst.*, vol. 55, no. 10, pp. 3349–3357, Nov. 2008.

[17] Y. C. Kang, S. H. Ok, S. H. Kang, and P. A. Crossley, "Design and evaluation of an algorithm for detecting current transformer saturation," *Proc. Inst. Elect. Eng., Gen. Transm. Distrib.*, vol. 151, no. 1, pp. 27–35, Jan. 2004.

[18] H. Dashti, M. Sanaye-Pasand, and M. Davarpanah, "Current transformer saturation detectors for busbar differential protection," in *Proc. 42nd Int. Universities Power Eng. Conf.*, Brighton, U.K., 2007, pp. 338–343.

[19] B. Kasztenny, E. Rosoiowski, M. Eukowicz, and J. Izykowski, "Current related relaying algorithms immune to saturation of current transformers," in *Proc.6th Int. Conf. Develop. Power Syst. Prot.*, Nottingham, U.K., 1997, pp. 265–368.

[20] F. Preisach, "Uber die magnetische nachwerikung," *Zeitschrift Phys.*, vol. B 94, pp. 227–302, 1935.

[21] M. S. Sachdev and M. A. Baribeau, "A new algorithm for digital impedance relays," *IEEE Trans. Power App. Syst.*, vol. PAS-98, no. 6, pp. 2232–2240, Nov./Dec. 1979.

[22] N. Locci and C. Muscas, "Hysteresis and eddy currents compensation in current transformers," *IEEE Trans. Power Del.*, vol. 16, no. 2, pp. 154–159, Apr. 2001.

[23] A. Rezaei-Zare, R. Iravani, M. Sanaye-Pasand, H. Mohseni, and S. Farhangi, "An accurate current transformer model based on Preisach theory for the analysis of electromagnetic transients," *IEEE Trans. Power Del.*, vol. 23, no. 1, pp. 233–242, Jan. 2008.

[24] J. Füzi, "Analytical approximation of Preisach distribution functions," *IEEE Trans. Magn.*, vol. 39, no. 3, pp. 1357–1360, May 2003.

[25] O. Henze and W. M. Rucker, "Identification procedures of Preisach model," *IEEE Trans. Magn.*, vol. 39, no. 2, pp. 833–836, Mar. 2002.

[26] E. Dlala, J. Saitz, and A. Arkkio, "Inverted and forward Preisach models for numerical analysis of electromagnetic field problems," *IEEE Trans. Magn.*, vol. 42, no. 8, pp. 1963–1973, Aug. 2006.

[27] S. K. Hong, H. K. Kim, and H. K. Jung, "Formulation of the verett function using least square method," *IEEE Trans. Magn.*, vol. 34, no. 5, pp. 3052–3055, Sep. 1998.

[28] E. Dlala, J. Saitz, and A. Arkkio, "Hysteresis modeling based on symmetric minor loops," *IEEE Trans. Magn.*, vol. 41, no. 8, pp. 2343–2348, Aug. 2005.

[29] D. H. Everett, "A general approach to hysteresis-Part 4: An alternative formulation of the domain model," *Trans. Faraday Soc.*, vol. 51, pp. 1551–1557, 1955.

[30] I. D. Mayergoyz, "Mathematical models of hysteresis," *IEEE Trans. Magn.*, vol. MAG-22, no. 5, pp. 603–608, Sep. 1986.

[31] T. Doong and I. D. Mayergoyz, "On numerical implementation of hysteresis models," *IEEE Trans. Magn.*, vol. MAG-21, no. 5, pp. 1853–1855, Sep. 1985.

[32] H. Hu, H. Zhang, and R. B. Mrad, "Preisach based dynamic hysteresis model," in *Proc. Int. Conf. Intelligent Mechatronics and Automation*, Chengdu, China, 2004, pp. 825–830.

[33] L. A. Kojovic, "Impact of current transformer saturation on overcurrent protection operation," in *Proc. IEEE Power Eng. Soc. Summer Meeting*, Canada, 2002, pp. 1078–1083.

[34] *For Harmonic Control in Electric Power Systems, Section 10.4 Current Distortion Limits*, IEEE Std. 519-1999.

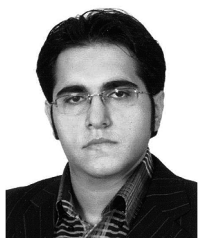

Firouz Badrkhani Ajaei received the B.Sc. degree in electrical engineering from The Amirkabir University of Technology (Tehran Polytechnic), Tehran, Iran, in 2006, and the M.Sc. degree from The University of Tehran, Tehran, in 2009.

His research interests include power system protection, power electronics, distributed generation, as well as analysis and simulation of electromagnetic transients in power systems and apparatus.

Majid Sanaye-Pasand (M'98–SM'05) received the B.Sc. degree in electrical engineering from The University of Tehran, Tehran, and the M.Sc. and Ph.D. degrees from The University of Calgary, Calgary, AB, Canada.

Currently, he is a Professor with the School of Electrical and Computer Engineering, University of Tehran. His research interests include power system protection, control, and transients.

Mahdi Davarpanah received the B.Sc. degree in electrical engineering from the Power and Water University of Technology, Tehran, Iran, in 2002 and the M.Sc. degree from The University of Tehran, Tehran, in 2005, where he is currently pursuing the Ph.D. degree.

His research interests include power system protection, distribution systems, and study and simulation of electromagnetic transients in power systems and apparatus.

Afshin Rezaei-Zare (M'08–SM'10) received the B.Sc., M.Sc., and Ph.D. degrees in electrical power engineering (Hons.) from The University of Tehran, Tehran, Iran, in 1998, 2000, and 2007, respectively.

From 2005 to 2007 and 2007 to 2009, he was a Visiting Scientist and a Postdoctoral Fellow at the Electrical and Computer Engineering Department, University of Toronto, Toronto, ON, Canada, respectively. From 2008 to 2009, he was a Consultant for AREVA NP Canada Ltd., focusing on the analysis of ferroresonance and switching overvoltages in power generation stations and 500 kV transmission systems. Currently, he is with the Department of Special Studies and Professional Development, Transmission System Development Division, Hydro One, Toronto, ON, Canada. His research interests include the analysis and modeling of electromagnetic transients in power systems and equipment, numerical solution techniques, modeling, analysis, and diagnostics of power transformers, as well as high-voltage phenomena and testing.

Dr. Rezaei-Zare is a registered Professional Engineer in the Province of Ontario, Canada.

Reza Iravani (M'85–SM'00–F'03) received the B.Sc. degree in electrical engineering from Tehran Polytechnic University, Tehran, Iran, in 1976, and the M.Sc. and Ph.D. degrees in electrical engineering from the University of Manitoba, Winnipeg, MB, Canada, in 1981 and 1985, respectively.

Currently, he is a Professor with the Department of Electrical and Computer Engineering, University of Toronto, Toronto, ON, Canada. His research interests include power electronics as well as power system dynamics and control.